

Baryon susceptibilities, nongaussian moments and the QCD critical point

Jiunn-Wei Chen^{1,2}, Jian Deng³ and Lance Labun²

¹ *Department of Physics and National Center for Theoretical Sciences,
National Taiwan University, Taipei, 10617 Taiwan*

² *Leung Center for Cosmology and Particle Astrophysics (LeCosPA)
National Taiwan University, Taipei, 10617 Taiwan*

³ *Key Laboratory of Particle Physics and Particle Irradiation (MOE),
School of Physics, Shandong University, Jinan 250100, China*

(Dated: 18 October, 2014)

We calculate model-independently the impact of the critical point on higher order baryon susceptibilities χ_n , showing how they depend on fluctuations of the order parameter. Including all tree level diagrams, we find new contributions to χ_4 equally important to the kurtosis of the order parameter fluctuations, and we characterize the kurtosis and other nongaussian moments as functions on the phase diagram. Important features of this analysis are then confirmed by a Gross-Neveu model study with good agreement with other model studies as well as lattice and experimental data. This suggests the universality of the characteristic peak in baryon susceptibilities as a signal of the critical point. We discuss leveraging measurements of different χ_n to extrapolate the location of the critical point.

A major goal of QCD theory and heavy-ion collision (HIC) experiment is to locate the critical end point in the chemical potential–temperature (μ – T) plane [1]. It is the target of the beam energy scan at RHIC and the future FAIR experiment, which are designed to create and measure QCD matter at high temperature and density. Lattice simulations are also developing methods to calculate properties of QCD matter at $\mu \neq 0$ [2, 3], which cannot be reached directly due to the sign problem.

The critical point itself is a second-order transition, characterized by diverging correlation length ξ , due to vanishing mass of the order parameter field σ . This fact, $m_\sigma^{-1} = \xi \rightarrow \infty$, is a statement about the two-point correlation function of the σ field, and we can use low energy effective field theory to relate other correlation functions to the critical point and phase structure. σ correlations influence observables such as baryon number fluctuations because the σ couples like a mass term for the baryons, meaning that the presence of σ changes the baryon energy [4]. Thus our aim is to establish the theory connection from the phase structure through σ dynamics to observables, here proton number fluctuations, which can be compared to event-by-event fluctuations in HICs [5, 6] and to lattice simulations [3].

It is important to keep in mind that the QCD matter created in HICs is dynamic. The measured data in general integrate properties from the initial state and expansion dynamics, and they may not represent equilibrium properties of QCD matter at the freeze-out μ, T , especially if the fireball has passed near the critical point [7]. Assuming the departure from equilibrium is small, we interpret the freeze-out data as approximate measurements of the phase diagram, which can be compared with theory and lattice predictions to help locate the critical point.

The fluctuation observables compared between HICs and lattice simulations are ratios of baryon susceptibili-

ties

$$m_1 = \frac{T\chi_3}{\chi_2}, \quad m_2 = \frac{T^2\chi_4}{\chi_2}, \quad \chi_n = \frac{\partial^n \ln \mathcal{Z}}{\partial \mu^n} \quad (1)$$

with the volume dependence eliminated in the ratios. More precisely, HICs measure proton fluctuations, which are shown to directly reflect the baryon fluctuations, because the order parameter field, the scalar σ , is an isospin singlet [8]. From here, one approach is model independent, considering the partition function as a path integral over σ , $\mathcal{Z} = \int \mathcal{D}\sigma e^{-\Omega[\sigma]/T}$, and the effective potential of the Landau theory $\Omega[\sigma]$ contains the phase structure in its coefficients. However those parameters are not determined by the theory. Previously this has been used to search for dominant contributions to χ_n close to the critical point [9, 10]. Another approach is to evaluate $\ln \mathcal{Z}$ in a QCD-like model, such as NJL [11], to gain predictive power of χ_n as functions on the phase diagram. We pursue both approaches to put the model independent results into the context of the global phase diagram.

We analyze a general polynomial form of the effective potential $\Omega[\sigma]$. We derive the χ_n as functions of the σ fluctuation moments $\langle \delta\sigma^k \rangle$, extracting new, equally important contributions to m_2 in addition to the σ field kurtosis κ_4 , studied by [10]. We show that negative κ_4 is restricted to the normal phase, and thus these new contributions are necessary to understand recent HIC and lattice results for m_2 . Our model independent results are corroborated with quantitative study of the 1+1 dimensional Gross-Neveu (GN) model, revealing remarkably good qualitative agreement with both other model studies [11] as well as the experimental data. This consistency suggests that those features of our findings are model-independent.

We begin with the effective potential for the order parameter field,

$$\Omega[\sigma] = \int d^3x \left(-J\sigma + \frac{g_2}{2}\sigma^2 + \frac{g_4}{4}\sigma^4 + \frac{g_6}{6}\sigma^6 + \dots \right) \quad (2)$$

with coefficients g_{2n} functions of temperature and chemical potential, determining the phase diagram. Focusing on long range correlations, we consider only the zero momentum $\vec{k} = 0$ mode, and so do not write the kinetic energy term $(\vec{\nabla}\sigma)^2$ here [9]. With the explicit symmetry breaking parameter $J \rightarrow 0$, the point where $g_2 = g_4 = 0$ is the tricritical point (TCP), separating the second order transition line for $g_4 > 0$ from the first order line for $g_4 < 0$. When $J \neq 0$, the second order line disappears into a crossover transition through which the σ minimum $\langle\sigma\rangle \equiv v$ changes smoothly as a function of temperature, and the TCP becomes a critical end point (CEP).

Fluctuations of the order parameter field obey an effective potential obtained by first minimizing the potential Eq. (2) and then Taylor expanding around v , yielding

$$\Omega[\delta\sigma] - \Omega_0 = \int d^3x \left(\frac{m_\sigma^2}{2} \delta\sigma^2 + \frac{\lambda_3}{3} \delta\sigma^3 + \frac{\lambda_4}{4} \delta\sigma^4 + \dots \right) \quad (3)$$

with $\delta\sigma(x) = \sigma(x) - v$. The constant $\Omega_0 \equiv \Omega[\sigma=v]$ does not influence the fluctuations, but does appear in the observables corresponding to the mean field contribution. The vev v satisfies the gap equation $v(g_2 + g_4 v^2 + g_6 v^4) = J$, and depends on μ, T through the g_{2n} .

Calculating μ -derivatives of the partition function gives an explicit relation between susceptibilities χ_n and $\delta\sigma$ fluctuations. Starting with the second order,

$$T^2 \chi_2 = T^2 \frac{\partial^2 \ln \mathcal{Z}}{\partial \mu^2} = -T \langle \Omega'' \rangle + \langle (\Omega')^2 \rangle - \langle \Omega' \rangle^2 \quad (4)$$

where $\langle f \rangle = \mathcal{Z}^{-1} \int \mathcal{D}\sigma f e^{-\Omega/T}$ is the expectation value of the function f including σ fluctuations. The prime indicates differentiation with respect to μ ,

$$\frac{\partial^k \Omega}{\partial \mu^k} = \int d^3x (a_{k0} + a_{k1} \delta\sigma + a_{k2} \delta\sigma^2 + \dots). \quad (5)$$

The first term a_{k0} is the mean-field contribution from differentiating Ω_0 . The linear term arises from the μ -dependence of the vev v .

Plugging these derivatives into Eq. (4), we keep all ‘‘tree-level’’ contributions, where the power of the correlator is less than or equal to order of the μ -derivative. This means that the expectation value of a product of correlators at different points is equal to the product of expectation values of correlators formed by making all possible contractions of $\delta\sigma$ at different points. The combination $\langle (\Omega')^2 \rangle - \langle \Omega' \rangle^2$ cancels disconnected diagrams. Applying these rules,

$$T^2 \chi_2 = -VT a_{20} + V^2 a_{11}^2 \langle \delta\sigma^2 \rangle \quad (6)$$

A diagrammatic method helps to organize these calculations and distinguish loops arising from contractions. So far Eq. (6) is just the usual second moment of particle number, here expanded in terms of the fluctuations of the $\delta\sigma$ field.

Applying this procedure, the higher order susceptibilities are

$$T^3 \chi_3 = -VT^2 a_{30} + 3V^2 T a_{11} a_{21} \langle \delta\sigma^2 \rangle - V^3 a_{11}^3 \langle \delta\sigma^3 \rangle - 6V^3 a_{11}^2 a_{12} \langle \delta\sigma^2 \rangle^2 \quad (7)$$

and

$$T^4 \chi_4 = -VT^3 a_{40} + V^2 T^2 (4a_{31} a_{11} + 3a_{21}^2) \langle \delta\sigma^2 \rangle - 6V^3 T a_{21} a_{11}^2 \langle \delta\sigma^3 \rangle + V^4 a_{11}^4 (\langle \delta\sigma^4 \rangle - 3\langle \delta\sigma^2 \rangle^2) - 12V^3 T (a_{22} a_{11}^2 + 2a_{21} a_{11} a_{12}) \langle \delta\sigma^2 \rangle^2 + 24V^4 (2a_{11}^2 a_{12}^2 + a_{11}^3 a_{13}) \langle \delta\sigma^2 \rangle^3 + 24V^4 a_{11}^3 a_{12} \langle \delta\sigma^3 \rangle \langle \delta\sigma^2 \rangle \quad (8)$$

Each factor of V comes from the d^3x integration in Eq. (5), and after inserting the expressions for $\langle \delta\sigma^k \rangle$, each $\chi_2, \chi_3, \chi_4 \propto V$. The fluctuation moments $\langle \delta\sigma^k \rangle$ are derived by functional differentiation of Eq. (3),

$$\kappa_2 = \langle \delta\sigma^2 \rangle = \frac{T}{V} \xi^2, \quad \kappa_3 = \langle \delta\sigma^3 \rangle = -2\lambda_3 \frac{T^2}{V^2} \xi^6 \quad (9)$$

$$\kappa_4 = \langle \delta\sigma^4 \rangle - 3\langle \delta\sigma^2 \rangle^2 = 6 \frac{T^3}{V^3} (2(\lambda_3 \xi)^2 - \lambda_4) \xi^8 \quad (10)$$

The point is that the a_{jk} coefficients weight how the $\delta\sigma$ correlations contribute to the higher order susceptibilities, χ_2, χ_3, \dots . Moreover, the a_{jk} have their own ξ dependence, which can be estimated analytically and model-independently, as well as compared with model studies. For example, we find that $a_{11} = m^2 \partial v / \partial \mu$ scales $\sim \xi^{-1}$ near the critical point. To compare to a given solvable model (such as the GN model below), the coupling constants $m_\sigma^2, \lambda_3, \lambda_4, \dots$ are calculated from the model’s effective potential and then their μ -derivatives evaluated yielding a_{kj} coefficients.

The third moment χ_3 has been studied in the NJL model and found to be negative around the phase boundary [11]. In agreement with power-counting ξ only in the $\delta\sigma$ correlators [9], the behavior of m_1 near the critical point can be explained by focusing on $\langle \delta\sigma^3 \rangle$ and hence the function $\kappa_3(\mu, T)$: In this case, estimating the ξ dependence of the a_{jk} coefficients in Eq. (7) reveals that the $a_{11}^3 \kappa_3$ term scales with the largest positive power of ξ .

However, for χ_4 there are many terms of the same (tree-level) order in the perturbation theory. Taking into account the ξ dependence of the coefficients, several contributions, including those represented by the diagrams in Fig. 1 scale with the same power of ξ as the κ_4 term. Although fewer σ propagators are visible in some of these diagrams, the coefficient functions a_{11}, a_{12} , and a_{13} all have important m_σ dependence. Looking at ξ -scaling, we find all three terms $\langle \delta\sigma^2 \rangle^2$, $\langle \delta\sigma^2 \rangle^3$, and $\langle \delta\sigma^2 \rangle \langle \delta\sigma^3 \rangle$ are approximately equally relevant as the κ_4 term. These analyses are supported by separately evaluating these terms in the GN model.

Next to see how the σ fluctuations are impacted by the CEP, we investigate $\kappa_3(\mu, T)$ and $\kappa_4(\mu, T)$ as functions

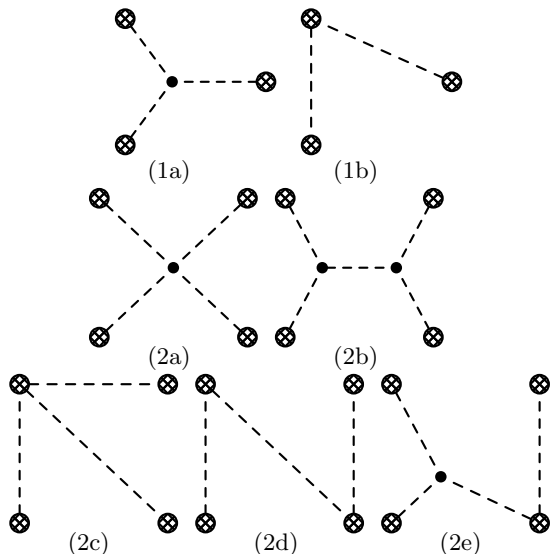


FIG. 1: Diagrams 1a,1b give leading contributions to χ_3 . Diagrams 2(a-e) are some of the leading contributions to χ_4 . Omitted are diagrams involving multiple μ derivatives at the same point.

on the phase diagram. With $J \rightarrow 0$, the unbroken phase is where $\langle \sigma \rangle = 0$, and in this case $\lambda_{2n} = g_{2n}$. Odd terms are zero, in particular $\lambda_3 \equiv 0$ in the unbroken phase, and negative κ_4 exists when $\lambda_4 = g_4 > 0$ above the second order phase transition line. In the symmetry broken phase,

$$2(\lambda_3 \xi)^2 - \lambda_4 = \frac{4}{\sqrt{D}} \left((g_4 - 2\sqrt{D})^2 + D \right), \quad (11)$$

$$D = g_4^2 - 4g_2g_6 > 0 \quad (J = 0)$$

D is the algebraic discriminant obtained when solving the gap question for the extrema, and it is positive in the broken phase, corresponding to real, nontrivial ($\sigma \neq 0$) solutions. Therefore, with $J = 0$, κ_4 is positive definite in the broken phase and the $\kappa_4 < 0$ region is defined by the conditions $g_2 > 0$ and $g_4 > 0$ occurring only in the unbroken phase. For concreteness, this is illustrated in the GN model, Figure 2.

Turning on $J \neq 0$ produces a continuous change in the λ_i . In particular, the $\kappa_4 = 0$ lines, bounding the $\kappa_4 < 0$ region, move continuously away from their $J = 0$ limits, and continue to obey the constraint “remembered” from $J = 0$ theory.

To see this, first recall that the tricritical point anchors one corner of the $\kappa_4 < 0$ region, and in the $J \neq 0$ theory, the critical end point continues to do so [10]. The reason is that κ_4 Eq. (9) has a local minimum where $\lambda_3 = 0$. For $J = 0$, $\lambda_3 = 0$ holds throughout the unbroken phase, but for any fixed $J \neq 0$, the relation $\lambda_3(g_2, g_4, \dots) = 0$ is an equation whose solution defines a line in the $\mu - T$ plane. The $\lambda_3 = 0$ line must pass through the critical end point. Differing trajectories of the phase boundary and $\lambda_3 = 0$ line are seen in the GN model, Figure 2.

The critical end point is located by the conditions $m_\sigma^2 = \lambda_3 = 0$, which means the coefficients g_{2n} satisfy [4]

$$g_2 = 5g_6v^4, \quad g_4 = -\frac{10}{3}g_6v^2, \quad v^5 = \frac{3}{8}\frac{J}{g_6} \quad @ \text{ CEP} \quad (12)$$

The vev $v = \langle \sigma \rangle$ is nonzero, as expected, and as the symmetry breaking is turned off $J \rightarrow 0$ these equations return to their $J = 0$ limits. Since $v^2 > 0$, the CEP always shifts to the “southeast”, into the fourth quadrant relative to the TCP of the $J = 0$ theory at $g_2 = g_4 = 0$.

To locate the $\lambda_3 = 0$ line, relax condition on m_σ^2 to find that $\lambda_3 = 0$ is the set of points satisfying

$$g_2 = \frac{7}{3}g_6v^4 + \frac{J}{v}, \quad g_4 = -\frac{10}{3}g_6v^2 \quad (13)$$

The $\lambda_3 = 0$ line leaves the CEP parallel to the first order line, and hence proceeds in the direction of decreasing g_4 . With $g_2 > 0$ and $g_4 < 0$ near the critical point (Eq. (12)), the relation Eq. (13) requires that v decreases along the $\lambda_3 = 0$ line. In the high T limit, $v \rightarrow 0$, so that the $\lambda_3 = 0$ line asymptotes to $g_4 = 0$ from below. Thus, from Eq. (13) we deduce that $\lambda_3 = 0$ typically cannot proceed close to the $\mu = 0$ axis, since that would require that the tricritical point of the $J = 0$ theory is near the $\mu = 0$ axis. The $\kappa_4 < 0$ -region must migrate toward higher T and μ with the critical end point.

In the high T , low μ behaviour of κ_4 is given by expanding for small v : $2(\lambda_3 \xi)^2 - \lambda_4 = -g_4 + 2\left(\frac{(3g_4)^2}{g_2} - 5g_6\right)v^2 + \mathcal{O}(v^4)$ which is valid where $g_2, g_4 > 0$, far away from the lines where g_2, g_4 vanish. Approaching from high T , κ_4 starts out negative just as in the $J = 0$ theory, and becomes positive just where the vev v becomes large enough that the second term starts to win over the first. Therefore, as the magnitude of explicit breaking increases enhancing the order parameter, the $\kappa_4 = 0$ line and $\kappa_4 < 0$ region move farther from the phase boundary.

We demonstrate the features derived above in the phase diagram and susceptibilities of the GN model. The fermion number susceptibilities behave very similarly to other models such as PNJL [12]. The GN model comprises N fermions in 1 spatial dimension with bare mass m_0 and a four-fermion interaction $\propto g^2$, and in the large N limit has a rich phase structure [13]. The physical mass m is given by $m\gamma = (\pi/Ng^2)m_0$ where $\gamma = \pi/(Ng^2) - \ln \Lambda/m$ is the parameter controlling the magnitude of explicit symmetry breaking. At small μ, T , there is a chiral condensate $\langle \bar{\psi}\psi \rangle$ and the order parameter is the effective mass $M = m_0 - g^2N\langle \bar{\psi}\psi \rangle$. The effective potential is a function of M , and we focus on the region above and on the low μ side of the critical point [13]

The phase diagram behaves as described model-independently: For $\gamma \rightarrow 0$, there is a tricritical point and second order line extending to the $\mu = 0$ axis. For $\gamma \neq 0$, the second order line vanishes into a crossover and the critical end point shifts increasingly to the “southeast” away from the former tricritical point. Figure 2 compares the phase diagrams of the GN model for $\gamma = 0$ and

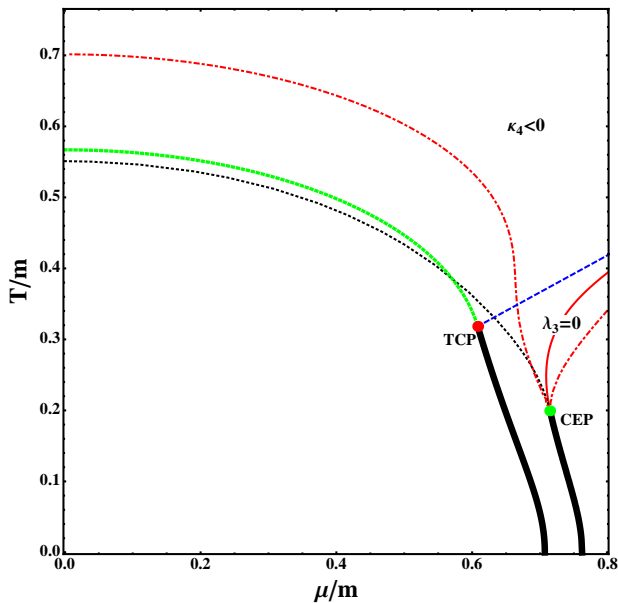


FIG. 2: Phase diagram of the GN model, with phase boundaries and TCP of the $\gamma = 0$ theory and the CEP of the $\gamma = 0.1$ theory. The $\kappa_4 < 0$ region of the $\gamma = 0$ is above the second order (green) line and left of the dashed (blue) line that joins the boundary at the TCP. The $\kappa_4 < 0$ region of the $\gamma = 0.1$ theory is delineated by the dot-dashed (red) line, and $\lambda_3 = 0$ the solid (red) line inside this region.

$\gamma = 0.1$. For $\gamma \neq 0$ the phase boundary is determined as the peak in the chiral susceptibility,

$$\chi_M = \frac{\partial \langle \bar{\psi} \psi \rangle}{\partial m} = \frac{1}{m} \left(M - T \frac{\partial M}{\partial T} - \mu \frac{\partial M}{\partial \mu} \right) \quad (14)$$

as is used in lattice QCD studies [14]. The phase boundary stays near the critical line of the $\gamma = 0$ theory, which is robust for different values of γ . All our results are shown in units of $m = 1$.

For $\gamma = 0$, the $\kappa_4 < 0$ region is delineated by the second-order line and the $g_4 = 0$ line. For $\gamma = 0.1$, it is delineated by the dot-dashed line with a cusp at the CEP. Varying γ , we see that the $\kappa_4 < 0$ region evolves continuously as a function of γ from its $\gamma \rightarrow 0$ limit. The $\lambda_3 = 0$ line leaves the CEP parallel to the first order line, and the $\kappa_4 < 0$ region is approximately symmetric around it very near the CEP. However, the $\lambda_3 = 0$ line then asymptotes to the $g_4 = 0$ line, which pulls the $\kappa_4 < 0$ region away from the phase boundary.

We plot m_2 on the phase diagram in Figure 3. The negative m_2 region forms a wedge opening up from the CEP and extends deeper across the phase boundary than the $\kappa_4 < 0$ region. Negative m_2 could be accessible to freeze-out at $\mu < \mu_{\text{CEP}}$, and the signature would be a minimum followed by a rapid increase to a positive peak, as seen in the (green) freeze-out curve closest to the phase boundary. Moving freeze-out progressively away from the phase boundary, both the minimum and maximum of m_2 decrease in magnitude. Thus it is possible m_2 is

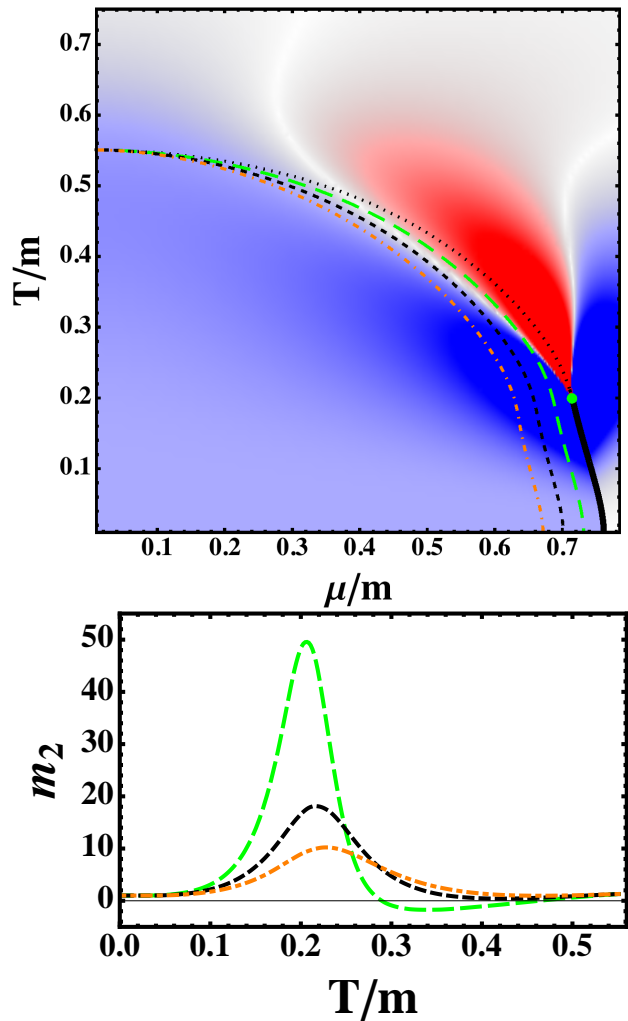


FIG. 3: Upper frame: Density plot of m_2 in the $\mu - T$ plane with $\gamma = 0.1$. The white lines indicate where $m_2 = 0$ and in the (red) wedge between these lines $m_2 < 0$. The first order line is the solid heavy line, and the crossover line is the dotted line, determined by the max of Eq. (14). The dashed lines are hypothetical freeze-out curves, color-coded to correspond to the lines in the lower frame.

only positive along the freeze-out curve (for example the lowest curve). Its maximum provides a residual signal of proximity to the CEP, seeing that the height of the peak decreases rapidly away from the phase boundary. Comparing upper and lower frames of Fig. 3, we see that the peak in m_2 is always at a temperature higher (or μ lower) than the CEP.

Strikingly, the black line is in good qualitative agreement with lattice and HIC results. However, non-monotonic behaviour of m_2 along a single freeze-out line is insufficient to establish proximity to the CEP. Many possible freeze-out curves can be drawn that cross several contours of constant m_2 twice, and each will display a local maximum of m_2 as a function of μ or the collision energy. For this reason, it will be important to combine several probes of the phase diagram, and one way to start

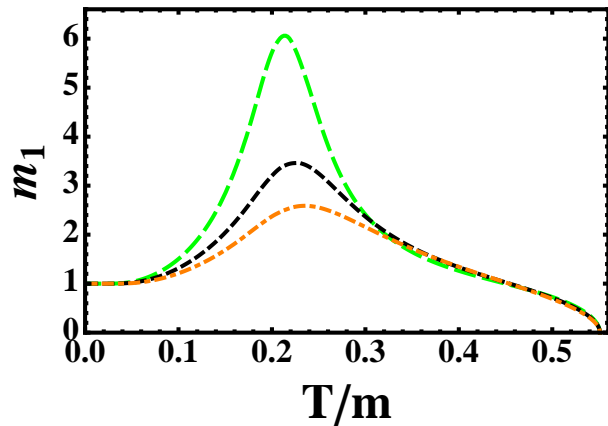


FIG. 4: m_1 along the hypothetical freeze-out lines given in the upper frame of Fig.3.

is to compare m_2 and m_1

In Figure 4, we plot m_1 along the same hypothetical freeze-out curves. Like m_2 it displays a positive peak close the CEP, and the magnitude of the maximum decreases for freeze-out lines farther away from the phase boundary. Again, the peak is at higher temperature (lower μ) than the CEP. This fact appears to be universal, as it is seen an Ising-model evaluation of κ_3 and κ_4 similar to [10]. Despite many similarities, the topography of the peaks in m_1 and m_2 differ in detail. Combining measurements of these two observables along the freeze-out curve, we may be able to extract more information about the CEP location.

To conclude, we have studied the fermion susceptibilities χ_2, χ_3, χ_4 analytically using a low energy effective theory for the order parameter field and numerically us-

ing the Gross-Neveu model as an example system. The model-independent analysis shows that larger quark mass pushes the critical end point to higher μ , and there are constraints on the position of the CEP relative to the tricritical point of the zero quark mass theory.

In agreement with previous work, nonmonotonic behaviour of m_1 and m_2 appears as a signal of the critical region in the phase diagram. Consistent with experimental data, we find m_2 first decreases as a function of chemical potential μ , which is a remnant of the $m_2 < 0$ region above the critical point. Seeing a large peak in m_2 at larger μ /smaller \sqrt{s} would support this explanation of the data. However, it is necessary to accumulate as much corroborating evidence as possible to preclude false positive, and we note in this same region, m_1 is also expected to peak and decrease again. The peaks in m_1, m_2 are typically not the point of closest approach, and the temperature of the peaks are ordered $T_{\max, m_1} > T_{\max, m_2} > T_{\text{CEP}}$, a fact which might be leveraged to indicate the location of the critical point.

To the extent that the fireball is near thermodynamic equilibrium at freeze-out, the model independent features we find can be compared to experiment. It may be possible to refine the predictions by taking into account expansion dynamics [7]. More information may be extracted from the experimental data by combining measurements of m_1 and m_2 along the single available freeze-out curve (and possibly other curves available from lattice).

Acknowledgments: JWC is supported in part by the MOST, NTU-CTS, and the NTU-CASTS of R.O.C. J.D. is supported in part by the Major State Basic Research Development Program in China (Contract No. 2014CB845406), National Natural Science Foundation of China (Projects No. 11105082).

-
- [1] M. A. Stephanov, PoS LAT **2006**, 024 (2006) [hep-lat/0701002]; K. Fukushima and C. Sasaki, Prog. Part. Nucl. Phys. **72**, 99 (2013) [arXiv:1301.6377 [hep-ph]]; S. Gupta, X. Luo, B. Mohanty, H. G. Ritter and N. Xu, Science **332**, 1525 (2011) [arXiv:1105.3934 [hep-ph]]; and references therein.
- [2] P. de Forcrand and O. Philipsen, Phys. Rev. Lett. **105**, 152001 (2010) [arXiv:1004.3144 [hep-lat]]; A. Li, A. Alexandru and K. F. Liu, Phys. Rev. D **84**, 071503 (2011) [arXiv:1103.3045 [hep-ph]].
- [3] R. V. Gavai and S. Gupta, Phys. Lett. B **696**, 459 (2011) [arXiv:1001.3796 [hep-lat]].
- [4] M. A. Stephanov, K. Rajagopal and E. V. Shuryak, Phys. Rev. Lett. **81**, 4816 (1998) [hep-ph/9806219]. M. A. Stephanov, K. Rajagopal and E. V. Shuryak, Phys. Rev. D **60**, 114028 (1999) [hep-ph/9903292].
- [5] M. M. Aggarwal *et al.* [STAR Collaboration], Phys. Rev. Lett. **105**, 022302 (2010) [arXiv:1004.4959 [nucl-ex]].
- [6] L. Adamczyk *et al.* [STAR Collaboration], Phys. Rev. Lett. **112**, 032302 (2014) [arXiv:1309.5681 [nucl-ex]].
- [7] B. Berdnikov and K. Rajagopal, Phys. Rev. D **61**, 105017 (2000) [hep-ph/9912274]. C. Nonaka and M. Asakawa, Phys. Rev. C **71**, 044904 (2005) [nucl-th/0410078]. C. Athanasiou, K. Rajagopal and M. Stephanov, Phys. Rev. D **82**, 074008 (2010) [arXiv:1006.4636 [hep-ph]].
- [8] Y. Hatta and M. A. Stephanov, Phys. Rev. Lett. **91**, 102003 (2003) [Erratum-ibid. **91**, 129901 (2003)] [hep-ph/0302002].
- [9] M. A. Stephanov, Phys. Rev. Lett. **102**, 032301 (2009) [arXiv:0809.3450 [hep-ph]].
- [10] M. A. Stephanov, Phys. Rev. Lett. **107**, 052301 (2011) [arXiv:1104.1627 [hep-ph]].
- [11] M. Asakawa, S. Ejiri and M. Kitazawa, Phys. Rev. Lett. **103**, 262301 (2009) [arXiv:0904.2089 [nucl-th]].
- [12] V. Skokov, B. Friman and K. Redlich, Phys. Lett. B **708**, 179 (2012) [arXiv:1108.3231 [hep-ph]].
- [13] O. Schnetz, M. Thies and K. Urlichs, Annals Phys. **321**, 2604 (2006) [hep-th/0511206].
- [14] Y. Aoki, Z. Fodor, S. D. Katz and K. K. Szabo, Phys. Lett. B **643**, 46 (2006) [hep-lat/0609068]. A. Bazavov, T. Bhattacharya, M. Cheng, *et al.* Phys. Rev. D **85**, 054503 (2012) [arXiv:1111.1710 [hep-lat]]. L. Levkova, PoS LATTICE **2011**, 011 (2011) [arXiv:1201.1516 [hep-lat]].